SCIENTIFIC REPORTS

OPEN

SUBJECT AREAS:
INORGANIC LEDS
NANOPARTICLES
NANOPHOTONICS AND PLASMONICS

Received
24 June 2014

Accepted
22 August 2014

Published
22 September 2014

Correspondence and requests for materials should be addressed to A.F. (afad@fotonik.dtu.dk)

Surface plasmon coupling dynamics in InGaN/GaN quantum-well structures and radiative efficiency improvement

Ahmed Fadil[1], Daisuke Iida[2], Yuntian Chen[3], Jun Ma[4], Yiyu Ou[5], Paul Michael Petersen[1] & Haiyan Ou[1]

[1]Department of Photonics Engineering, Technical University of Denmark, 2800 Lyngby, Denmark, [2]Department of Applied Physics, Tokyo University of Science, Katsushika, 125-8585 Tokyo, Japan, [3]School of Optical and Electronic Information, Huazhong University of Science and Technology, 430074 Wuhan, China, [4]Institute of Semiconductors, Chinese Academy of Sciences, 100083 Beijing, China, [5]Light Extraction ApS, 2800 Lyngby, Denmark.

Surface plasmonics from metal nanoparticles have been demonstrated as an effective way of improving the performance of low-efficiency light emitters. However, reducing the inherent losses of the metal nanoparticles remains a challenge. Here we study the enhancement properties by Ag nanoparticles for InGaN/GaN quantum-well structures. By using a thin SiN dielectric layer between Ag and GaN we manage to modify and improve surface plasmon coupling effects, and we attribute this to the improved scattering of the nanoparticles at the quantum-well emission wavelength. The results are interpreted using numerical simulations, where absorption and scattering cross-sections are studied for different sized particles on GaN and GaN/SiN substrates.

InGaN/GaN based light-emitting diodes (LED) have proven to be an efficient light source in the visible spectral region, thanks to its widely tunable bandgap. The external quantum efficiency of this material system at blue emission wavelengths reaches above 80%[1], however, in moving towards green, yellow and red wavelengths by increasing the indium (In) composition the efficiency is decreased. This is due to the increased piezoelectric field which induces the quantum-confined stark effect and thereby limiting the internal quantum efficiency (IQE)[2]. Several approaches have been researched to improve the device efficiency. One way is to improve the light extraction efficiency (LEE), achieved through nanostructuring the crystal surface. Approaches include designing photonic crystal structures to inhibit light propagation in the lateral direction and controlling the emission pattern[3], nanopillar[4] and nanodome structures[5,6], and surface roughening[7]. Another quantity that can be improved to enhance the device efficiency is the IQE. A first approach to achieve this is by improving the crystal quality at the growth process[8,9]. It is also reported that strain relaxation occurs during formation of nanopillars through the active region, whereby the IQE is improved[10].

In the last ten years surface plasmonics have been heavily researched as a way to improve the IQE of InGaN/GaN emitters by the so-called Purcell effect, where the spontaneous recombination rate is enhanced. Energy coupling from excitons in InGaN/GaN quantum-well (QW) active region into surface plasmon polariton (SPP) modes of Ag thin films has been demonstrated[11,12]. The energy out-coupling of these SPP modes into photons was later demonstrated through photoluminescence (PL) enhancement[13,14]. Randomly distributed metal nanoparticles (NPs) have also been investigated as a way to improve the recombination rate through exciton coupling with localized surface plasmon (LSP) modes[15–20]. The advantage of LSP modes comes from fact that they do not require a phase-matching condition in order to radiate the stored energy[21]. Creating a periodic structure of NPs has the additional advantage of allowing control over interparticle spacing and resonance wavelength tuning, giving a higher degree of optimization[22–24].

In most works where metal NPs are used to improve the emitter efficiency through LSP coupling, focus has been on matching the emission wavelength with the LSP resonance of NPs. The objective being that at resonance wavelength the coupling will be strongest. Since LSP resonance depends on metal NP size, much effort has been put into controlling the NP size to match the resonance wavelength with that of the emission[16,20,21]. The resonance is either estimated through the transmittance, reflectance or extinction spectrum. These measurement techniques do however include the contribution from the absorption inside the NPs, from which it is difficult to interpret whether the resonance is absorption or scattering dominated. It is therefore seen in some reported cases that PL enhancement is weakened or even suppressed when the resonance wavelength is near the emission wave-

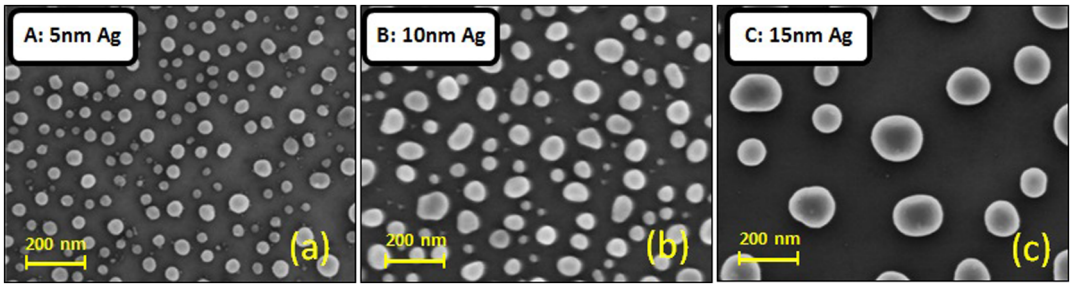

Figure 1 | **Scanning electron microscope (SEM) images of self-assembled Ag NPs, with pre-annealed Ag film thickness of (a) 5 nm, (b) 10 nm and (c) 15 nm.**

length[20,22]. The major figure of merit of the metallic NPs is to capture the emission from the active layer, and subsequently redirect the stored energy in the LSP resonance into the freely propagating photons, coined as the LSP radiative efficiency. However, certain fraction of energy will be dissipated inside the metal as heating losses, which is related to the absorption cross-section of the NP in the context of light scattering. On the other hand, the scattering cross-section will be an estimation of the particles efficiency in radiating the stored energy, which is required to maximize to achieve a better light extraction.

In this work we have studied the scattering and LSP coupling dynamics of Ag NPs on InGaN/GaN QW structures, and the mechanisms behind PL suppression and enhancement. Randomly self-assembled Ag NPs are fabricated and a dielectric layer of SiN between Ag and GaN surface is employed to modify the LSP mode for the investigations. PL and absorption spectra are obtained to characterize the samples. 3D finite-different time-domain (FDTD) simulations are implemented to calculate cross-sections and field enhancement factors of a single Ag NP on GaN/SiN substrate. The effects of particle diameter and SiN thickness variation are studied. By comparing the simulated and experimental results, we manage to give a detailed description of LSP-QW coupling and LSP radiation mechanism of Ag NPs on InGaN/GaN QW structures.

Results

The samples are InGaN/GaN QW structures grown on c-plane double side polished sapphire substrate, where the active region consists of 5 periods of GaN (12 nm)/InGaN (2 nm) QWs, together with a capping layer of 30 nm GaN to define the distance between the last QW and the top surface. A thin dielectric layer of SiN was then deposited on some of the samples using plasma-enhanced chemical vapor deposition (PECVD), with a deposition thickness of 15 and 120 nm. To fabricate Ag NPs, a thin layer of Ag was e-beam evaporated on the samples followed by a rapid thermal annealing process forming self-assembled particles. The different Ag film thicknesses used were 5, 10 and 15 nm, and the sizes of Ag NPs depended on this pre-annealed film thickness as shown in Figure 1. The three different Ag NP distributions are denoted as A, B and C, referring to 5, 10 and 15 nm annealed films, respectively. Each distribution is fabricated on samples with 0, 15 and 120 nm SiN layer, constituting nine samples in total (A1-3, B1-3 and C1-3). The average particle diameter of sample A, B and C is approximately 50, 110 and 160 nm, respectively.

For PL measurements, the excitation and detection is done from the polished sapphire side as sketched in Figure 2(a). The PL spectra are plotted in Figure 2(b). For each three cases of different SiN thickness, the reference has the same SiN thickness but does not have Ag NPs. This is to exclude the PL enhancement from the dielectric layer itself. The PL spectra with Ag NPs are normalized to the peak value of its corresponding reference. For samples without SiN we observe an integrated PL enhancement of a factor 2.4 with sample C1, while sample B1 shows an almost unchanged PL spectrum. Sample A1 which has the smallest Ag NP size distribution shows PL suppression.

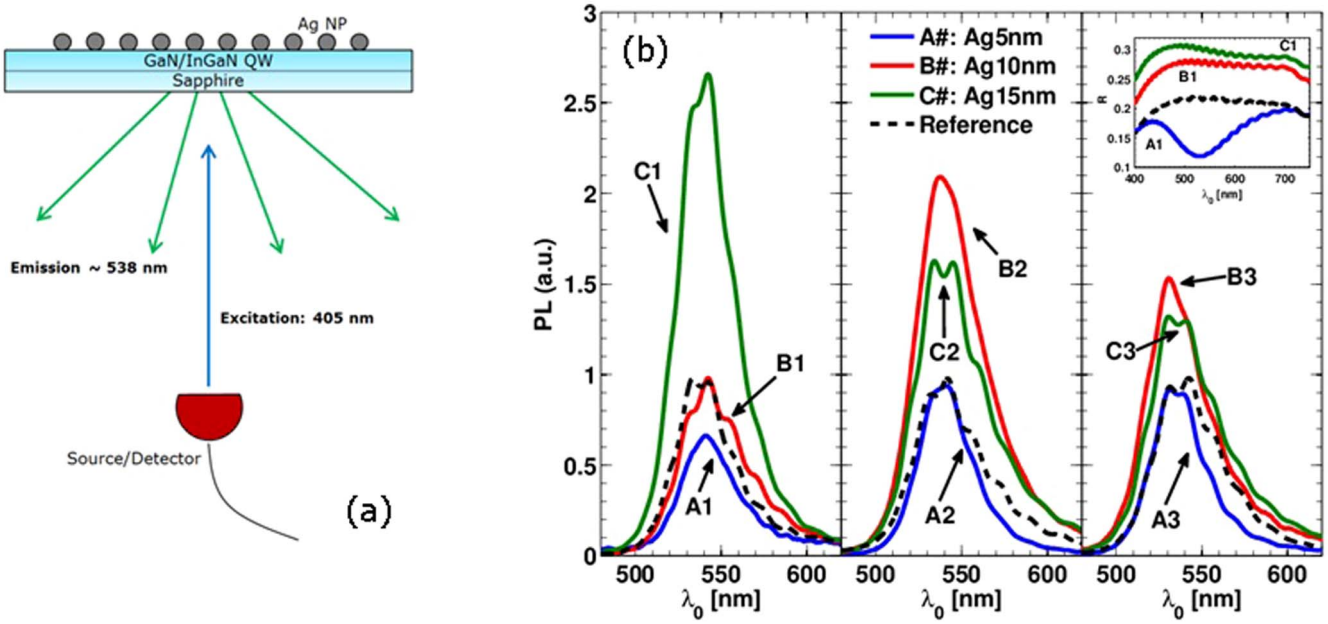

Figure 2 | (a) PL measurement setup. (b) Reflectance corrected PL spectra of nine samples with Ag NPs and three references without Ag NPs. Inset shows the reflectance spectra of A1, B1 and C1.

The metal NPs can induce an increased back reflection of both the excitation laser and the QW emission at the substrate-metal interface, which will cause an additional PL enhancement unrelated to SP enhancement. However, it has been confirmed through IQE, time-resolved PL, and electroluminescence (EL) measurements, that an enhancement due to metal NPs based on this excitation and detection scheme can indeed be attributed to LSP-QW coupling[13–19,22–23]. Nonetheless it is still required to exclude the contribution from the enhanced reflection of the excitation source due to Ag NPs as done in Ref. 22, as well as the enhanced reflection at the emission wavelength. The inset of Figure 2(b) shows the reflectance spectrum, where it is seen that samples B1 and C1 have an enhanced reflectance of nearly a factor of 1.5. The reflectance spectra of the remaining samples, A2-3, B2-3 and C2-3 show a similar trend as A1, B1 and C1. The absorbed excitation intensity in the QWs is roughly assumed to be proportional to the incident plus the reflected intensity at excitation wavelength, i.e. $1 + R$. If the inclusion of Ag NPs increases the reflectance from R to R_{Ag}, the absorption will be increased by a factor $f_{refl} = (1+R_{Ag})/(1+R)$. To exclude reflectance enhancement effects the PL spectra of B1-3 and C1-3 has been divided by a factor of $K = f_{refl}R_{enh}$, where $R_{enh} = R_{Ag}/R$ is the enhancement at emission wavelength and R is the reference sample reflectance. In Figure 2(b) the PL correction factor K has already been taken into account and the observed PL enhancements can therefore be attributed to LSP-QW coupling.

Interestingly the situation is drastically affected by the inclusion of a SiN layer. We observe that with 15 nm SiN the integrated PL enhancement of sample C2 is reduced to 1.8. This is in agreement with the expectation that coupling strength is reduced with increasing distance between QWs and Ag NPs[13]. However, the opposite trend is seen for sample B2, which displays an integrated PL enhancement of a factor of 2.1. The situation of sample A2 also shows improvement, in the sense that the PL is not suppressed as it was for A1, although the PL of A2 is still not enhanced relative to the reference.

We also observe that with a 120 nm SiN layer Ag NPs still manage to result in a PL enhancement, even though the distance between NPs and QW active region is greatly increased. The integrated PL enhancement factors of samples B3 and C3 are 1.6 and 1.5, respectively.

To obtain further insight on the LSP resonances of the Ag NPs, the normalized absorption spectra were obtained from transmittance and reflectance spectra as shown in Figure 3 for samples without SiN and with 15 nm SiN. It is clearly noticed for samples A1-2 and B1-2, that the LSP absorption peaks blue-shift as the SiN is included. A strong and well-defined absorption peak was not visible for C1 and C2.

When designing for SP enhancement using metal NPs the usual strategy is to compare and match the LSP resonance peak with the emission wavelength, where the LSP resonance is estimated through a dip in the reflectance or transmittance spectrum[16–19,22–24]. It is expected that SP enhancement of InGaN/GaN QWs is optimized by matching the resonance and emission wavelengths. We are, however, observing a situation where a strong PL enhancement is obtained for sample C1 despite the absence of a well-defined absorption peak. Although samples A1 and B1 have well-defined resonance peaks near the emission wavelength, no PL enhancement is obtained. To clarify these ambiguities in our experiments, as well as previous observations, we need to quantify the two competing factors, i.e. light scattering (or re-emission) and absorption in the excitation of LSP resonances. A measurement of the reflectance and transmittance spectra reveals information about the absorption of NPs, and this is subtly related to the LSP resonance and LSP-QW coupling. Essentially, it is the competing effect between scattering and absorption that ultimately determines the optimal efficiency of plasmon mediated light emitting devices. This scattering, which is related to the radiative efficiency of LSP resonances, determines the SP

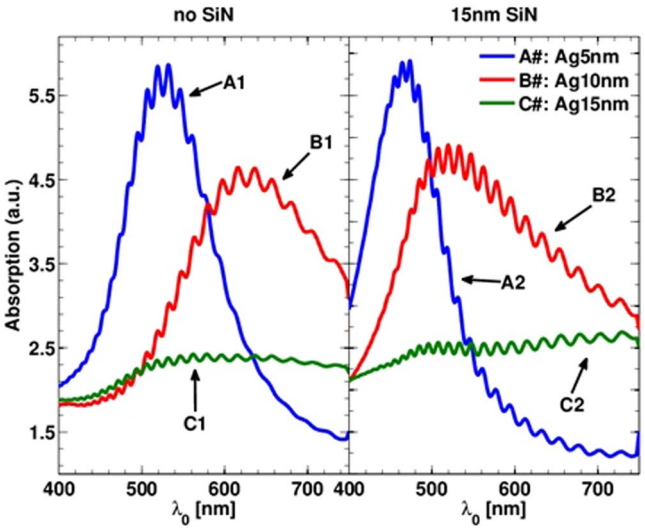

Figure 3 | Normalized absorption spectra for samples without and with 15 nm SiN between GaN and Ag NPs.

enhancement properties of metal NPs. By only considering the absorption spectrum it is not possible to conclude that an absorption peak spectrally aligned with the emission wavelength can result in an enhancement through LSP-QW coupling.

To understand the observed measurements, we conducted 3D FDTD simulations to investigate the absorption and scattering properties of Ag NPs on GaN/SiN substrate. As seen from Figure 1 the particle size distribution and interparticle spacing are randomly distributed around an average value, and simulating a large ensemble of randomly distributed NPs with an acceptable accuracy would require relatively large computational resources. However, if we assume that the interaction between the Ag NPs is weak and neglectable when interacting with light, it will be sufficient to simulate a single Ag NP. By modelling a single NP we can obtain the properties of an ensemble of non-interacting NPs. The results will help us gain a qualitative understanding of the observed measurements. We have not simulated a periodical arrangement of NPs to avoid grating effects and resonances which are not present in a random distribution[25]. In the simulations the NPs are assumed to have the shape of a spherical dome. The size variations seen in the SEM images of Figure 1 are simulated through separate instances by a diameter sweep. The variation of the optical properties with the diameter will give us an understanding of how such an ensemble of non-interacting particles with varying sizes respond to light illumination. The Ag NP height is set to $H = \alpha D/2$, where D is the NP diameter, and $\alpha = 1.8$ is a fixed aspect ratio.

Figure 4(a) shows the absorption cross-sections σ_{abs} for particle diameters of $D = 50$, 110 and 160 nm (D50, D110 and D160), without and with 15 nm SiN layer, where comparisons are to be made with samples A1-2, B1-2 and C1-2, respectively. In agreement with experimental measurements, we observe a blue-shift of the absorption peak when including SiN for D50 and D110. The observed peak is the LSP mode which is confined at the substrate-metal interface. Another feature consistent with the measurements is the fact that for D50 and D110 the spectrum shows a well-defined absorption peak as is the case for the Ag NPs of samples A1-2 and B1-2. The simulations of D160 also reveal that the absorption spectra of large NPs do not show a well-defined peak, which is consistent with the absorption measurement of the Ag NPs on samples C1-2. There is an apparent disagreement when considering the absorption strengths, where the strongest absorption occurs for samples A1-2, which for the simulations corresponds to D50. However, it should be noted that the particle density (particles per unit area) increases with decreasing

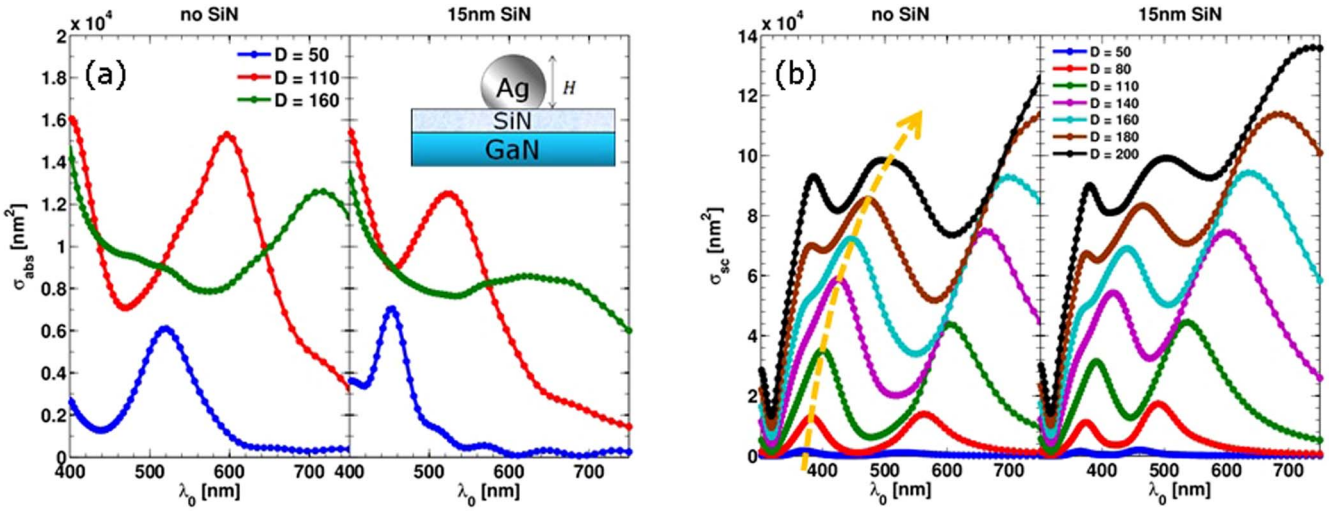

Figure 4 | Simulation results of a single Ag NP on GaN/SiN substrate. (a) Absorption cross-sections at three diameters. (b) Scattering cross-section spectra for different NP diameters. The arrow shows the direction of increasing diameter D and position of a higher order LSP mode.

particle size, such that samples A1-2 has the highest density, and C1-2 has the lowest density as seen in Figure 1. With a larger number of particles, the absorption would correspondingly be higher. Therefore even though the single particle absorption strength of samples A1-2 according to simulations should be lower than B1-2 and C1-2, the larger density of particles on sample A1-2 would in total result in larger absorption than B1-2 and C1-2.

Figure 4(b) shows the scattering cross-sections σ_{sc} for particles of various diameters. As mentioned, scattering is the significant parameter when considering SP enhancement of InGaN/GaN QWs through LSP-QW coupling, and here we see that increasing the particle size (D) increases the scattering, which is a well-known result in the dipole approximation[21]. The simulations also reveal a red-shift of the resonance peak with increasing diameter. For diameters larger than $D = 160$ nm a higher order scattering mode is seen to emerge and red-shift with increasing size, the position of which is noted by the arrow. The peak of the higher-order mode for largest particle is located around 500 nm, which is below the emission wavelength. Another point to note is the fact that a well-defined scattering resonance peak exists despite its absence in the absorption cross-section spectrum, as is the case for D160 with 15 nm SiN.

Considering the increasing scattering cross-section with increasing particle size, we can partially understand how a PL enhancement can be obtained in the case of samples C1-3. The absence of a resonance peak at the emission wavelength is not equivalent to the absence of LSP scattering. This is evident from Figure 4(b), where if we consider the sample of diameter $D = 160$ nm, we notice that its scattering cross-section values throughout the whole wavelength range from 400 to 750 nm, even in the valleys, exceed the peak scattering cross-section value of the sample with $D = 110$ nm for the 15 nm SiN case. This means that even at off-resonance conditions large Ag NPs have strong scattering capabilities, which is a requirement for SP enhancement.

From the PL measurements in Figure 2(b), it was noticed that the PL suppression in case of sample A1 was neutralized by the inclusion of SiN. This can be understood when considering the fact that the absorption peak is blue-shifted away from the emission peak. In Figure 5(a) we have the simulation result of absorption cross-section variation with particle diameter on different substrates. The absorption peak around $D = 80$ nm is seen to be shifted towards $D = 110$ nm by including SiN, resulting in a reduced absorption below 80 nm. This can explain why the inclusion of SiN neutralized the PL suppression for sample A1 with average Ag NP size around 50 nm, as seen for A2-3.

To understand the behavior of samples B1-3 and C1-3 when going from a GaN to GaN/SiN substrate, we consider the scattering cross-section variation with diameter in Figure 5(b). The essential feature to notice here is the increased scattering from around 90 to 180 nm diameter when a 15 nm thick SiN slab is included, resulting in an increase of the scattering by a factor of 3.1 and 1.6 at $D = 110$ and 160 nm, respectively. To also take into account the effects of absorption we consider the scattering-to-extinction ratio σ_{sc}/σ_{ext}, where $\sigma_{ext} = \sigma_{abs} + \sigma_{sc}$. This parameter qualitatively reveals if a NP of a given size is scattering ($> 1/2$) or absorption dominated ($< 1/2$) in itself. This is shown in the inset of Figure 5(b), where the dashed horizontal line at 0.5 is the value at which the absorption and scattering are equal. Without SiN the scattering-to-extinction ratio at $D = 110$ nm is 0.56, implying a relatively large dissipation compared to the scattering by Ag NPs of the given size. With a SiN layer the ratio is increased by 40% for $D = 110$ nm. While the scattering-to-extinction ratio for the sphere $D = 160$ nm increases moderately, i.e. by a factor of 9.8% with inclusion of SiN slab. Considering the PL measurements of samples B1-2, we therefore believe that the increased scattering is the mechanism behind the increased PL intensity from B1 to B2 when the SiN layer is introduced. The scattering-to-extinction ratio also reveals that for $D = 50$ nm, the value is below 0.5 regardless of SiN layer, which implies an absorption dominated operation for such small NPs. The SiN does however increase the ratio from 0.17 to 0.40, implying a decreased dissipation relative to the scattering. We may now understand how there can be an improvement in the PL intensity when going from A1 to A2 relative to the reference, when including the SiN layer, although no PL enhancement is observed.

The scattering results of Figure 5(b) can explain why sample B1-2 has an improved PL intensity with 15 nm SiN, but does not explain why the PL enhancement of sample C2 is reduced compared to C1, and exceeded by sample B2. The scattering and absorption cross-sections of Ag NP reveal information about the radiative efficiency of the LSP mode, but it does not tell us anything about the energy transfer or coupling between LSP-QW. To investigate this coupling, we will consider the field intensity enhancement $|E|^2$ in the plane of the QWs due to the Ag NP. This parameter will correspond to the decay rate enhancement of optical emitters positioned in the near-field of a metal NP[26]. In the simulations with a single Ag NP we calculate the average intensity enhancement over an area of $1.5D \times 1.5D$ at the plane of the QWs below the NP. The results are shown in Figure 6(a), where the intensity enhancement spectra of three different sized particles are shown on three different substrates. As a comparison we have Figure 6(b) which shows the PL ratio between

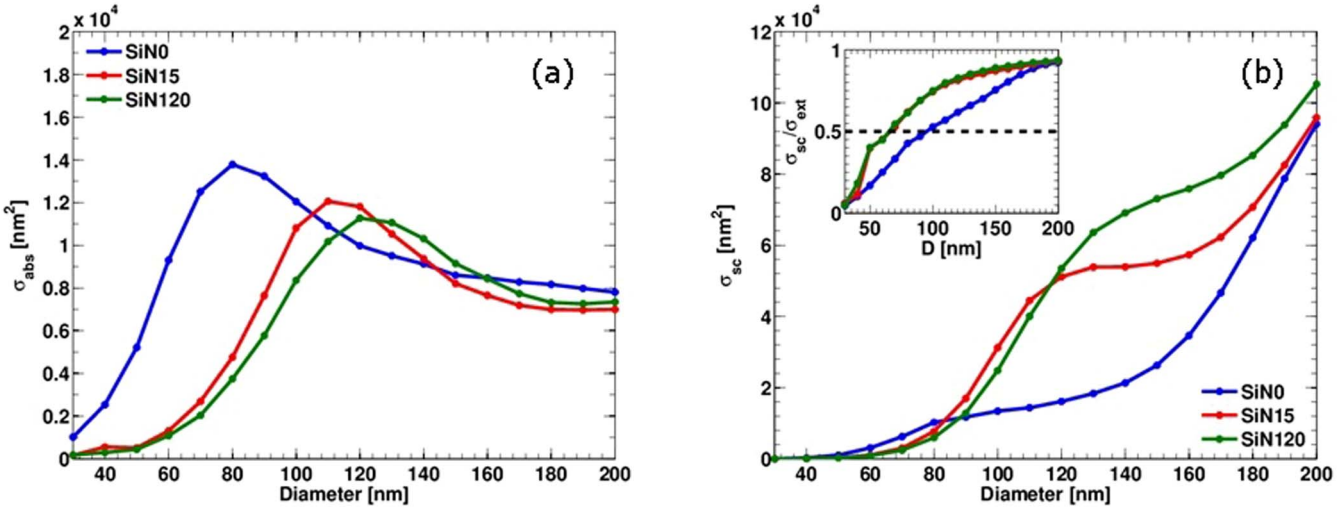

Figure 5 | (a) Absorption and (b) scattering cross-section variation with particle diameter at $\lambda_0 = 538$ nm. The inset shows the scattering to extinction ratio. The substrates are GaN (SiN0), 15 nm and 120 nm SiN on GaN (SiN15 and SiN120).

the samples with Ag NPs and the reference from the experimental results of Figure 2.

The situation without SiN of Figure 6(a) shows that the field enhancement factor for an Ag NP of diameter $D = 160$ nm exceeds that of a diameter $D = 110$ nm in a range from about 460 to 560 nm. With 15 nm SiN the D110 particle has a higher field enhancement factor than D160 in the range from 510 to 610 nm. The field enhancement spectrum is related to the scattering cross-section and hence also affected by the blue-shift of the peak scattering due to SiN. Although the peak enhancement of D110 is reduced, it is nonetheless shifted towards the emission peak of the QWs. It is also noticed that for wavelengths above 610 nm, the enhancement of D160 nm starts to exceed that of D110 with 15 nm SiN. This appears to be closely related to the scattering peak being located near 635 nm for D160, though the peak enhancement is located at about 680 nm. When considering the 120 nm SiN layer, the distance between the Ag NP and the QW region is 150 nm, and yet still there is a small field enhancement up to a factor of 1.5 remaining for D110 and D160. Around the emission peak the enhancement is once more higher for D110 than for D160.

Comparing now with the experimental results in Figure 6(b), we observe a similar trend with the PL ratios, where the PL enhancement of sample B2 exceeds that of sample C2 close to the emission peak, when using 15 nm SiN. The peak of sample C2 PL ratio is likely to have originated from a Fabry-Perot oscillation feature in the PL signals. Nonetheless, for wavelengths above 600 nm the PL enhancement of C2 is higher than that of B2, which is a similar situation to that seen from the simulations in Figure 6(a) with 15 nm SiN. For the samples with 120 nm SiN a relatively large enhancement factor of nearly 1.5 is present for B3 and C3. The feature which is roughly captured by simulations is the stronger PL enhancement of sample B3 relative to sample C3 for wavelengths near and below the emission peak, while the PL enhancement of sample C3 dominates at longer wavelengths.

To summarize the above results, we consider the intensity enhancements at the emission wavelength, 538 nm, and its variation with particle diameter as shown in Figure 7. With only a GaN substrate (SiN0), the peak enhancement is located around $D = 180$ nm. By including the SiN layer the peak is shifted to around $D = 100$ nm, irrespective of the SiN thickness. The point which is reiterated is that particles with D around 110 nm have an improved field intensity enhancement with a thin SiN layer (SiN15) compared to bare GaN substrate (SiN0), while particles with D around 160 nm have a degraded enhancement. It is now possible to understand the PL

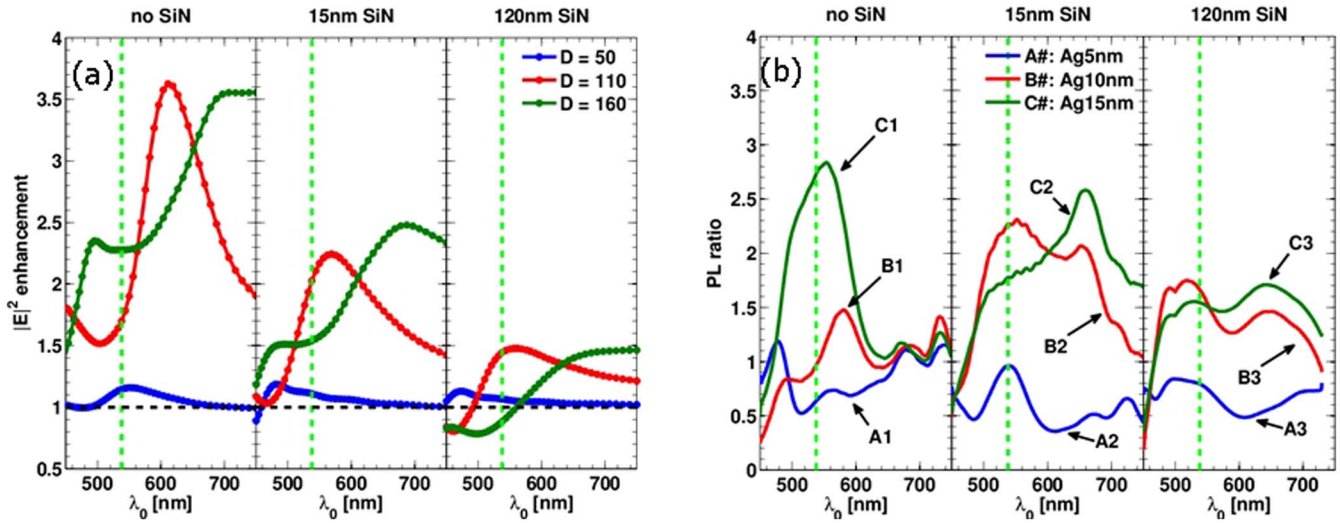

Figure 6 | (a) Intensity enhancement spectrum by Ag NP on GaN/SiN substrate. (b) PL ratio of the measurements in Figure 2. The vertical lines show the position of the emission peak at 538 nm.

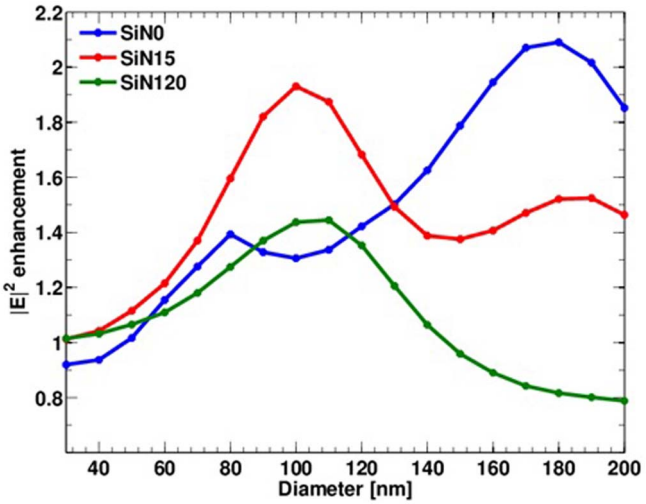

Figure 7 | Intensity enhancement variation with Ag NP diameter at 538 nm wavelength on different substrates.

results of Figure 2(b), where sample C1 has the strongest enhancement without SiN, while sample B2 dominates with SiN and sample C2 is degraded relative C1. Even though we only considered a single Ag NP, the simulations nonetheless qualitatively explained the measurements. The validity of this estimation holds if we neglect the interactions between the different Ag NPs on our samples. The accuracy of this approximation is further improved by the fact that the Ag NPs have random variation in size and position, which means that we do not have any grating-like effects, such as a strong particle interaction and grating modes. We believe that the single NP model does well in explaining the observed trends in our measurements qualitatively. Using this simple model we have managed to understand how the PL enhancement of the samples (B1-3) with average Ag NP size around 110 nm can be improved by including a SiN layer when considering scattering and absorption cross-sections of Ag NPs of a similar size. Through the results of figures 5 and 7 we have managed to obtain consistent explanations and conclusions about our measured results.

Discussion

In summary we have investigated the effects of SP enhancement using different sized Ag NPs on different substrates. By including a 15 nm SiN layer, we found an improvement of the PL intensity for samples with small sized NPs. This could be explained by an improved scattering and LSP resonance blue-shift of the NPs when the substrate was modified. We have found that what is important to consider when working with metal NPs for SP enhancement, is not only the absorption dip in the transmittance or reflectance spectra, but rather the combined effects of absorption, scattering, scattering-to-extinction ratio, and field enhancement. It is relatively easy to obtain metal NPs with resonances matching the emission wavelength, but it does not ensure SP enhancement of the optical emitter if the NPs cannot scatter the stored energy efficiently. Using a simplified modelling of Ag NPs we could reasonably explain the observed measurements, and we found that in order to improve the efficiency of the QW structure through LSP coupling the metal NPs should have a large scattering-to-extinction ratio. This could be achieved by either increasing the NP size or by modifying the environment of the NPs, i.e. including a SiN layer on GaN.

Methods

Fabrication. InGaN/GaN QW structures were grown by metalorganic vapor phase epitaxy (MOVPE) on C-plane sapphire substrates. The final epi-structure consisted of a 2 μm thick GaN layer, a 10 period InGaN (3 nm)/GaN (2 nm) superlattice layer, a 5 period GaN (11.5 nm)/InGaN (2 nm) QW active region covered with 30 nm thick GaN capping layer. The distance of last QW to LED surface was 30 nm. A thin film layer of Si_3N_4 was deposited on the GaN surface using plasma-enhanced chemical vapor deposition (PECVD). The obtaining layer thicknesses were 15 and 120 nm. Following the dielectric layer deposition, Ag thin films of 5, 10 and 15 nm thickness were deposited using electron-beam evaporation. Self-assembled Ag NPs were then formed through a rapid thermal annealing process at 350°C for 30 min in N_2 atmosphere.

Characterization. For the PL measurements a sapphire side excitation and detection setup was used, with an excitation laser at 405 nm wavelength. The diffuse and specular parts of the transmittance and reflectance spectra were measured, following which the absorption could then be obtained. The absorption normalization is relative to the reference sample without Ag NPs.

Simulation. For the FDTD simulations, experimental values for the metal permittivity of Ag were used[27], and the refractive index of GaN and SiN was set to 2.43 and 1.9, respectively. The intensity enhancement calculations were done in the plane of the QWs, 25 nm below the GaN interface. The intensity was averaged over an area of dimension $1.5D \times 1.5D$, to keep a fixed ratio between the particle cross-section and the area over which to calculate the field enhancement.

1. Narukawa, Y., Ichikawa, M., Sanga, D., Sano, M. & Mukai, T. White light emitting diodes with super-high luminous efficacy. *J. Phys. D. Appl. Phys.* **43**, 354002 (2010).
2. Takeuchi, T. *et al.* Quantum-Confined Stark Effect due to Piezoelectric Fields in GaInN Strained Quantum Wells. *Jpn. J. Appl. Phys.* **382**, L382 (1997).
3. Wierer, J. J., David, A. & Megens, M. M. III-nitride photonics-crystal light-emitting diodes with high extraction efficiency. *Nat. Photonics* **3**, 163–169 (2009).
4. An, H., Sim, J. I., Shin, K. S., Sung, Y. M. & Kim, T. G. Increased Light Extraction From Vertical GaN Light-Emitting Diodes With Ordered, Cone-Shaped Deep-Pillar Nanostructures. *IEEE J. Quantum Electron.* **48**, 891–896 (2012).
5. Zhao, P. & Zhao, H. Analysis of light extraction efficiency enhancement for thin-film-flip-chip InGaN quantum wells light-emitting diodes with GaN micro-domes. *Opt. Express* **20**, A765–76 (2012).
6. Ee, Y. *et al.* Optimization of Light Extraction Efficiency of III-Nitride LEDs With Self-Assembled Colloidal-Based Microlenses. *IEEE J. Sel. Top. Quantum Electron.* **15**, 1218–1225 (2009).
7. Fujii, T. *et al.* Increase in the extraction efficiency of GaN-based light-emitting diodes via surface roughening. *Appl. Phys. Lett.* **84**, 855 (2004).
8. Iida, D. *et al.* Analysis of strain relaxation process in GaInN/GaN heterostructure by in situ X-ray diffraction monitoring during metalorganic vapor-phase epitaxial growth pss. **214**, 211–214 (2013).
9. Yamamoto, T. *et al.* In situ X-ray diffraction monitoring of GaInN/GaN superlattice during organometalic vapor phase epitaxy growth. *J. Cryst. Growth* **393**, 108–113 (2014).
10. Dong, P. *et al.* Optical properties of nanopillar AlGaN/GaN MQWs for ultraviolet light-emitting diodes. *Opt. Express* **22**, A320 (2014).
11. Gontijo, I., Boroditsky, M. & Yablonovitch, E. Coupling of InGaN quantum-well photoluminescence to silver surface plasmons. **60**, 564–567 (1999).
12. Neogi, A. *et al.* Enhancement of spontaneous recombination rate in a quantum well by resonant surface plasmon coupling. *Phys. Rev. B* **66**, 1–4 (2002).
13. Okamoto, K. *et al.* Surface-plasmon-enhanced light emitters based on InGaN quantum wells. *Nat. Mater.* **3**, 601–5 (2004).
14. Okamoto, K. *et al.* Surface plasmon enhanced spontaneous emission rate of InGaN/GaN quantum wells probed by time-resolved photoluminescence spectroscopy. *Appl. Phys. Lett.* **87**, 071102 (2005).
15. Yeh, D.-M., Chen, C.-Y., Lu, Y.-C., Huang, C.-F. & Yang, C. C. Formation of various metal nanostructures with thermal annealing to control the effective coupling energy between a surface plasmon and an InGaN/GaN quantum well. *Nanotechnology* **18**, 265402 (2007).
16. Yeh, D.-M., Huang, C.-F., Chen, C.-Y., Lu, Y.-C. & Yang, C. C. Localized surface plasmon-induced emission enhancement of a green light-emitting diode. *Nanotechnology* **19**, 345201 (2008).
17. Huang, C.-W. *et al.* Fabrication of surface metal nanoparticles and their induced surface plasmon coupling with subsurface InGaN/GaN quantum wells. *Nanotechnology* **22**, 475201 (2011).
18. Cho, C.-Y. *et al.* Surface plasmon-enhanced light-emitting diodes using silver nanoparticles embedded in p-GaN. *Nanotechnology* **21**, 205201 (2010).
19. Kwon, M.-K., Kim, J.-Y. & Park, S.-J. Enhanced emission efficiency of green InGaN/GaN multiple quantum wells by surface plasmon of Au nanoparticles. *J. Cryst. Growth* **370**, 124–127 (2013).
20. Jiang, S. *et al.* Resonant absorption and scattering suppression of localized surface plasmons in Ag particles on green LED. *Opt. Express* **21**, 12100–12110 (2013).
21. Maier, S. A. *Plasmonics: Fundamentals and Applications.* (Springer, 2007).
22. Henson, J. *et al.* Enhanced near-green light emission from InGaN quantum wells by use of tunable plasmonic resonances in silver nanoparticle arrays. *Opt. Express* **18**, 21322–9 (2010).
23. Henson, J., DiMaria, J., Dimakis, E., Moustakas, T. D. & Paiella, R. Plasmon-enhanced light emission based on lattice resonances of silver nanocylinder arrays. *Opt. Lett.* **37**, 79–81 (2012).

24. Chen, H.-S. *et al.* Surface plasmon coupled light-emitting diode with metal protrusions into p-GaN. *Appl. Phys. Lett.* **102**, 041108 (2013).
25. Lamprecht, B. *et al.* Metal nanoparticle gratings: influence of dipolar particle interaction on the plasmon resonance. *Phys. Rev. Lett.* **84**, 4721–4 (2000).
26. Biteen, J. S. *et al.* Plasmon-Enhanced Photoluminescence of Silicon Quantum Dots: Simulation and Experiment. *J. Phys. Chem. C* **111**, 13372–13377 (2007).
27. Palik, E. D. *Handbook of Optical Constants of Solids.* (Academic, 1997).

Acknowledgments

This research was supported by the Danish Council for Strategic Research (0603-00494B).

Author contributions

A.F. and H.O. wrote the main manuscript. J.M. contributed to the processing and experimental measurements. D.I. grew the InGaN/GaN QW samples. Y.C. contributed to the interpretation of the numerical simulations. Y.O., P.P. and H.O. supervised the study.

Additional information

Competing financial interests: The authors declare no competing financial interests.

How to cite this article: Fadil, A. *et al.* Surface plasmon coupling dynamics in InGaN/GaN quantum-well structures and radiative efficiency improvement. *Sci. Rep.* **4**, 6392; DOI:10.1038/srep06392 (2014).